Progress In Electromagnetics Research, Vol. 123, 337–354, 2012

IMPROVED PERFORMANCE OF CIRCULARLY POLARIZED ANTENNA USING SEMI-PLANAR CHIRAL METAMATERIAL COVERS

D. Zarifi*, H. Oraizi, and M. Soleimani

Antenna and Microwave Research Laboratory, Iran University of Science and Technology, Tehran 1684613114, Iran

Abstract—The influence of semi-planar chiral metamaterial (CMM) structures on the important characteristics of circularly polarized (CP) antennas is investigated in this paper. Based on this idea, CP planar two-arm Archimedean spiral (ARSPL) antenna and helical antenna are designed and the effects of chiral covers on their gain (or directivity), axial-ratio (AR), and return loss are considered. The results demonstrate that this method is greatly effective and the addition of a semi-planar CMM cover at an optimized distance over the CP antenna, significantly improves its gain and axial ratio.

1. INTRODUCTION

Recently, metamaterials (MTMs) exhibiting interesting and unique properties nonexistent in natural materials have attracted increasing attention. The early prominent MTM structures had negative index of refraction. Remarkably, the negative index MTMs can be achieved by both negative permittivity and negative permeability in the same spectral region, which show the best performance, i.e., lower losses. Many applications have been proposed for MTMs, such as the interesting applications in antenna structures for miniaturization [1–4], bandwidth enhancement and directive emission [5–13]. An attractive category of MTMs known as the zero-index materials exhibit a considerable influence on the wave propagation and in increasing the directivity of dipole, linearly polarized microstrip, and linearly polarized horn antennas [14].

In 2003, the possibility of realizing negative refraction by chiral nihility was discussed [15]. In fact, chiral nihility is a special case

Received 5 November 2011, Accepted 19 December 2011, Scheduled 29 December 2011
* Corresponding author: Davoud Zarifi (zarifi@iust.ac.ir).

of chiral media which several applications have been proposed for it [16–23]. Afterwards, the general conditions to realize negative refraction chiral metamaterials (CMMs) were investigated and it was shown that negative refraction can be realized in CMMs having strong chirality, with neither negative permittivity nor permeability [24]. Although, natural chiral materials have very weak chirality, but properly designed CMM structures with considerable chirality can realize negative refractive index for either right circularly polarized (RCP) or left circularly polarized (LCP) waves. This property is the most manifest difference between CMMs and double-negative MTMs exhibiting negative refractive indices for linearly polarized waves. Recently, several theoretical [25, 26] and experimental studies on CMMs and their interesting applications have been proposed, such as negative refraction index [27–33], ultrathin linear polarization rotators [27–34], circular polarizer [35], focusing of electromagnetic waves [36–38], wide angle and polarization independent absorbers [39], and cloaking [40, 41].

This paper presents gain enhancement and axial ratio (AR) improvement techniques for circularly polarized (CP) antennas based on the utilization of semi-planar CMM covers as a novel application of CMM structures.

2. CHIRAL METAMATERIAL STRUCTURES

The constitutive equations for chiral media assuming a time harmonic dependence $e^{-j\omega t}$ are given by [42, 43]:

$$\mathbf{D} = \varepsilon\varepsilon_0\mathbf{E} + j\kappa\sqrt{\varepsilon_0\mu_0}\mathbf{H}, \quad \mathbf{B} = -j\kappa\sqrt{\varepsilon_0\mu_0}\mathbf{E} + \mu\mu_0\mathbf{H}, \tag{1}$$

where ε_0 and μ_0 are the permittivity and permeability of vacuum, and ε and μ are the relative permittivity and permeability of the chiral medium, and κ is the so-called chirality parameter. With this extraordinary constitutive relationship, chiral media have two important properties. The first one is optical (or electromagnetic) activity, which can rotate the polarization plane of a linearly polarized wave propagating through it. The second property is circular dichroism, which is attributed to the different absorptivity of a RCP and LCP polarized wave inside chiral medium. The wave equation in an isotropic chiral medium is:

$$\nabla^2\mathbf{E} + 2\frac{\kappa\omega}{c_0}\nabla\times\mathbf{E} + \frac{\omega^2}{c_0^2}(\mu\varepsilon - \kappa^2)\mathbf{E} = 0 \tag{2}$$

where c_0 and ω are the speed of light in vacuum and the angular frequency, respectively. It can be seen that the RCP and LCP waves

are the eigenpolarization of the wave equation. The refractive indices for the RCP (+) and LCP (−) waves are [42]:

$$n_{\pm} = n \pm \kappa \tag{3}$$

where $n = \sqrt{\varepsilon\mu}$. Both RCP and LCP waves have the same impedance given by $z/z_0 = \sqrt{\mu/\varepsilon}$ where z_0 is the impedance of free space. Given a large enough chirality, the negativity of refractive index for one of the circularly polarized wave is possible. Based on this concept, several semi-planar CMM structures have been proposed and demonstrated to achieve strong optical activity, circular dichroism, and negative refractive index, such as twisted rosettes [27], twisted crosses [28], twisted U-shaped Split Ring Resonators (U-SRRs) [29], double layer CMM structure [30], conjugated gammadion [31], complementary CMM structure [32], and L-shaped resonators CMM structure [33].

The four-fold rotational symmetry and lack of any mirror symmetry are inherent properties of aforementioned designs consisting of multiple layers of twisted copper patterns printed on dielectric boards. Owing to the missing four-fold rotational symmetry and linear birefringence, no optical activity is observable. Therefore, in order to obtain pure optical activity both chiral symmetry and four-fold rotational symmetry have to be present.

The parameter retrieval process of macroscopic electromagnetic (EM) parameters for a semi-planar CMM is generally the same as regular MTMs. However, due to the chiral nature of medium and different interactions among its chiral particles and RCP and LCP waves, it is somewhat more complicated [44]. In fact, the circularly polarized transmission coefficients ($T_{\pm}$), and reflection coefficients ($R_{\pm}$) of RCP and LCP waves should be measured. For simplicity, a linearly polarized EM wave (first, electric field in the x and then in the y direction) is incident on the CMM structure and the linear transmission coefficients, T_{xx}, T_{yx}, T_{yy}, and T_{xy}, and the linear reflections, R_{xx}, R_{yx}, R_{yy}, and R_{xy}, are measured, where the first subscript indicates the transmitted (reflected) field polarization (x- or y-polarized), and the second indicates the incident field polarization. Then, the linearly polarized transmissions and reflections should be converted to circular transmission coefficients (T_{++}, T_{+-}, T_{-+}, T_{--}) and reflection coefficients (R_{++}, R_{+-}, R_{-+}, R_{--}), where the first subscript indicates the transmitted (reflected) field polarization (RCP or LCP), and the second indicates the incident field polarization. Consider the RCP and LCP plane waves with unity amplitude, $E^{\pm} = (1/2)E_0(\hat{x} \mp j\hat{y})$, and defining the linear and circular transmission matrices as:

$$\begin{pmatrix} E_x^t \\ E_y^t \end{pmatrix} = \begin{pmatrix} T_{xx} & T_{xy} \\ T_{yx} & T_{yy} \end{pmatrix} \begin{pmatrix} E_x^i \\ E_y^i \end{pmatrix}, \quad \begin{pmatrix} E_+^t \\ E_-^t \end{pmatrix} = \begin{pmatrix} T_{++} & T_{+-} \\ T_{-+} & T_{--} \end{pmatrix} \begin{pmatrix} E_+^i \\ E_-^i \end{pmatrix}, \tag{4}$$

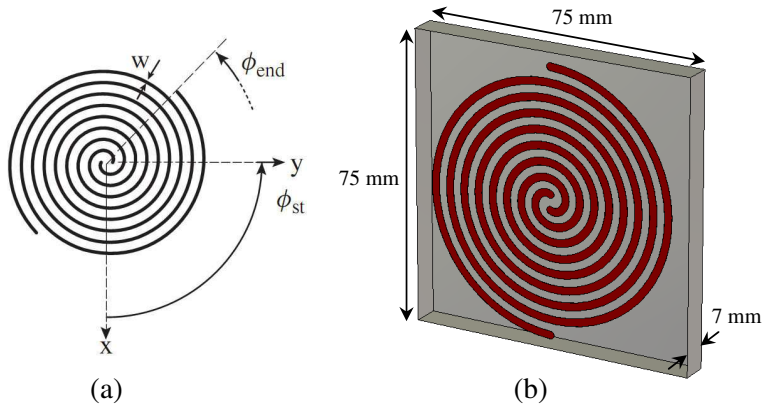

Figure 1. (a) Dimensions of the ARSPL antenna. (b) Configuration of the designed cavity backed ARSPL antenna.

where i and t subscripts indicate the incident and transmitted waves, respectively. Then, it can be easily shown that the circular scattering coefficients are converted from the linear scattering coefficients using the following equation:

$$\begin{pmatrix} T_{++} & T_{+-} \\ T_{-+} & T_{--} \end{pmatrix} = \frac{1}{2}\begin{pmatrix} 1 & +j \\ 1 & -j \end{pmatrix}\begin{pmatrix} T_{xx} & T_{xy} \\ T_{yx} & T_{yy} \end{pmatrix}\begin{pmatrix} 1 & 1 \\ -j & +j \end{pmatrix}$$
$$= \frac{1}{2}\begin{pmatrix} (T_{xx}+T_{yy})-j(T_{xy}-T_{yx}) & (T_{xx}-T_{yy})+j(T_{xy}+T_{yx}) \\ (T_{xx}-T_{yy})-j(T_{xy}+T_{yx}) & (T_{xx}+T_{yy})+j(T_{xy}-T_{yx}) \end{pmatrix}, \quad (5)$$

where T can be also replaced with R.

3. TWO-ARM ARCHIMEDEAN SPIRAL ANTENNA WITH TWISTED CROSSES CMM COVER

3.1. Antenna Design

The configuration of the two-arm Archimedean spiral (ARSPL) antenna is shown in Figure 1(a). The radial distance from the origin to a point on each arm of the antenna is [45]:

$$\begin{cases} r = a_{\mathrm{AR}}\phi, & \phi_{st} \le \phi \le \phi_{end} \\ r = a_{\mathrm{AR}}(\phi - \pi), & \phi_{st} + \pi \le \phi \le \phi_{end} + \pi \end{cases} \quad (6)$$

where $a_{\mathrm{AR}} = 1.273$, $\phi_{st} = 0.5\pi$, $\phi_{end} = 8.5\pi$, $w = 2\,\mathrm{mm}$. In order to obtain a unidirectional beam, a metallic cavity with dimensions of $75\,\mathrm{mm} \times 75\,\mathrm{mm} \times 7\,\mathrm{mm}$ is placed at the back of ARSPL antenna as shown in Figure 1(b). However, this cavity deteriorates the radiation

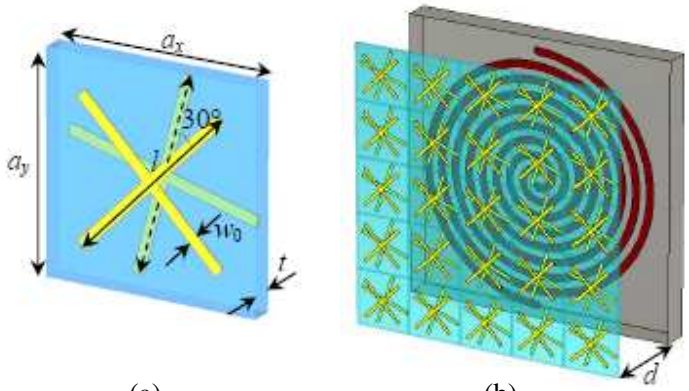

(a) (b)

Figure 2. (a) Unit cell of twisted crosses structure with the geometric parameters of $a_x = a_y = 15\,\text{mm}$, $l = 14\,\text{mm}$, $w_0 = 0.7\,\text{mm}$ and $t = 1.6\,\text{mm}$. (b) Configuration of the cavity backed ARSPL antenna with the twisted crosses CMM cover.

characteristics of antenna, which may be improved by an absorber strip (ABS) with $\varepsilon_r = 1.1$, $\sigma = 0.1\,\text{S/m}$, and internal radius of 29 mm and height of 7 mm attached to the vertical walls of the cavity (is not shown in figure).

3.2. Twisted Crosses CMM Cover

The design of bilayer cross-wires or twisted crosses as semi-planar CMM structure is already published [28]. The unit cell of this CMM structure is constructed by two copper cross-wires with width $w_0 = 0.7\,\text{mm}$ and length $l = 14\,\text{mm}$ printed on the opposite sides of an FR-4 board with dielectric constant 4.5, dielectric loss tangent 0.025, and thickness $t = 1.6\,\text{mm}$, as shown in Figure 2(a). Numerical simulations are executed in a frequency range of 2 to 12 GHz by using the unit cell template and frequency domain solver of CST Microwave Studio. Using a standard parameter retrieval method [44], the real and imaginary parts of $n_\pm$ are calculated and illustrated in Figure 3. According to these results and the near zero real and imaginary parts of n_+, it is expected that the application of this semi-planar CMM structure as a cover for a RCP antenna at frequency of about 6.7 GHz, the antenna directivity increases significantly due to the focusing effect. Note that these retrieved results are valid for a very large cover consisting of many unit cells. However, due to the physical constraints, the transverse dimensions of the practical covers should be finite and

in the order of antenna size. Therefore, the retrieved results should be considered as an initial value for an optimization process in order to achieve the optimum radiation characteristics.

3.3. Simulated Results

A 5×5 array of twisted crosses unit cells is placed above ARSPL antenna with spacing d, as shown in Figure 2(b). The transverse

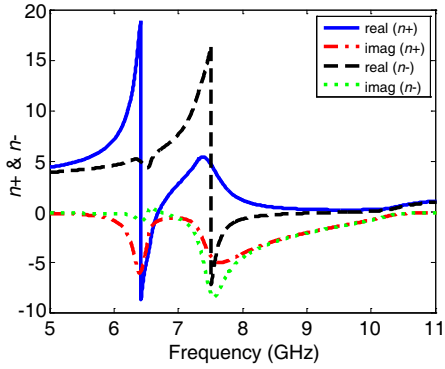

Figure 3. The real and imaginary parts of the RCP and LCP refractive indices for the twisted crosses CMM structure.

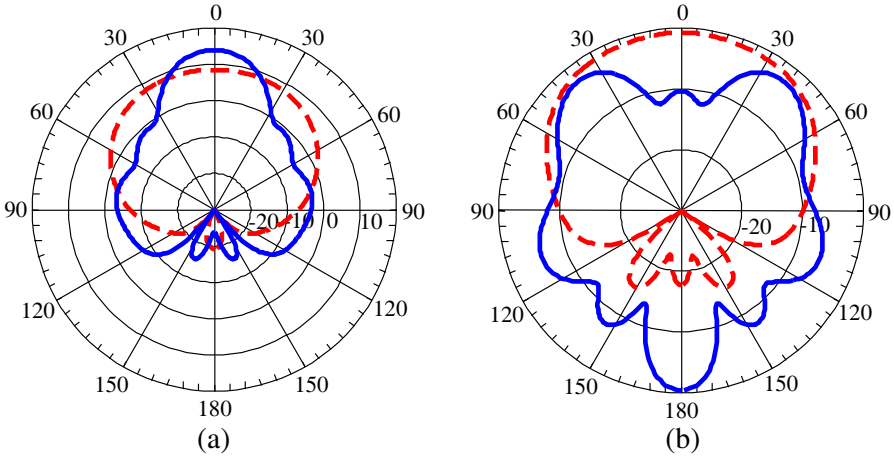

Figure 4. The radiation patterns (in dB) of cavity backed ARSPL antenna at frequency of 5.9 GHz with (solid line) and without (dashed line) cover in $\varphi = 0^\circ$ plane. (a) RHCP. (b) LHCP.

dimensions of the cover and conducting cavity are equal. Numerical simulations performed in a frequency range of 5.5 GHz to 7 GHz show that the optimum value of d is about 26 mm. In this case, the RCP gain of ARSPL antenna with cover approaches 14 dB at frequency 5.9 GHz, while the common antenna without cover has a gain of 8.6 dB. Theoretically, the maximum gain (or directivity) of an aperture antenna with the same transverse dimensions as ARSPL antenna is $4\pi A/\lambda^2 = 14.44$ dB. Therefore, the gain of ARSPL antenna with CMM cover has almost approached the theoretical limit of antenna gain with the same size and operating frequency. The radiation patterns in the $\varphi = 0^\circ$ plane at 5.9 GHz for the ARSPL antenna with and without CMM cover are shown in Figure 4. The radiation patterns in $\varphi = 0^\circ$ and $\varphi = 90^\circ$ planes are almost the same. Observe that the RCP gain of ARSPL antenna with CMM cover is about 24 dB higher than its LCP gain in the boresight direction ($\theta = 0^\circ$). Also, the placement of CMM cover on ARSPL antenna causes the half power beam width (HPBW) to decrease from 87° to 24° and the side lobe level (SLL) to increase from -28 dB to -18 dB.

The simulated RCP gain, AR in the boresight direction ($\theta = 0^\circ$), and S_{11} of ARSPL antenna (with feed impedance of 150 Ω) with and without CMM cover in the frequency range from 5.9 GHz to 6.5 GHz are shown in Figure 5, where the effects of placing CMM cover on the ARSPL antenna with absorbing strip (ABS) are also shown. Observe that the RCP gain of ARSPL antenna with CMM cover is increased by about 3.5–5.4 dB and AR and return-loss are considerably improved in this range. Furthermore, the AR of ARSPL antenna with both cover and the absorbing strip is less than 1 dB, which is an excellent property of the CP antenna. However, utilizing an absorbing strip in conducting cavity of ARSPL antenna (and absorption of energy in the cavity) causes some degradation of antenna gain. Further studies show that with increasing the transverse dimensions of cavity, the side lobe levels of radiation patterns are considerably reduced.

4. TWO-ARM ARCHIMEDEAN SPIRAL ANTENNA WITH DENDRITIC FRACTAL CMM COVER

4.1. Dendritic Fractal Cover Design

As mentioned before, the retrieved electromagnetic parameters of the semi-planar CMM structures are only valid for a rather large array consisting of many unit cells, while the sizes of antenna and its cover are finite. To rectify this problem, the miniaturized semi-planar CMM structures having smaller unit cells can be utilized.

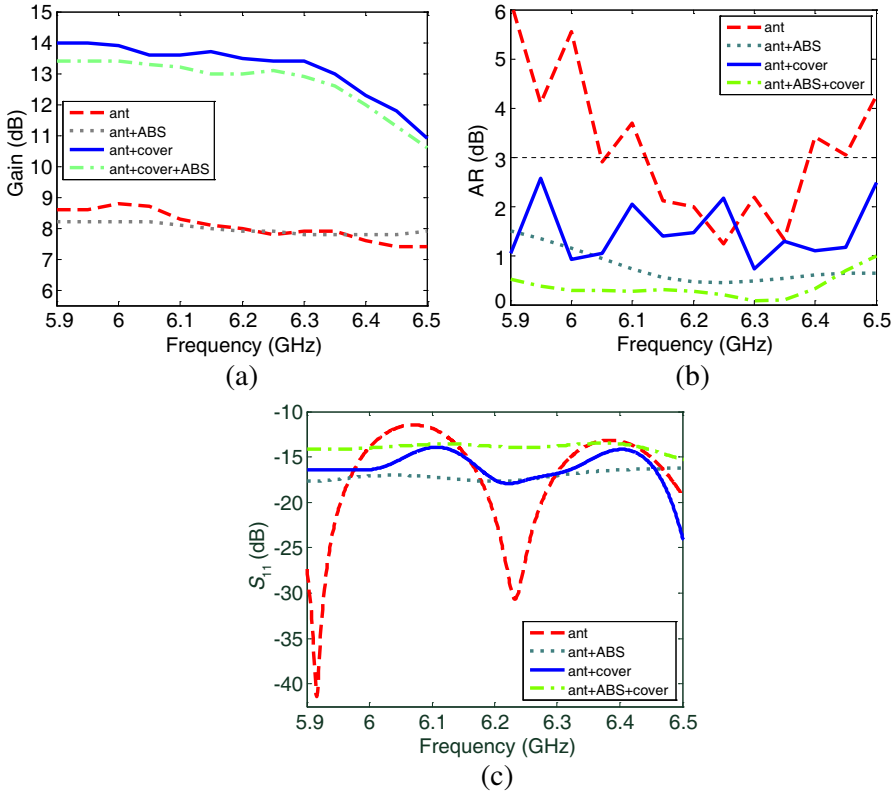

Figure 5. (a) The simulated RCP gain, (b) the AR, and (c) S_{11} of the cavity backed ARSPL antenna with and without the twisted crosses CMM cover. The simulated results of ARSPL antenna with ABS strip are presented.

One type of simple fractal geometry that can be utilized to increase the length of wires and miniaturize the structure is the dendritic fractal geometry. This fractal structure is generated by an iterative sequence to the starting simple wire structure. In the first iteration, the top segment of this wire is split at an almost optimized angle, $\theta = 60°$. As the iterative process continues, the end segment of each branch splits into two branches. The unit cell of dendritic fractal CMM structure is shown in Figures 6(a), (b). The lengths of straight sections in any arm of this structure correspond to the ratios of 1/2, 1/4, 1/8, 1/16, 1/16 and the transverse dimension of aggregate unit cells equal to 15 mm × 15 mm. With planar scaling (in x-y plane) of proposed structure with scale factor 0.6 and simulating in a frequency

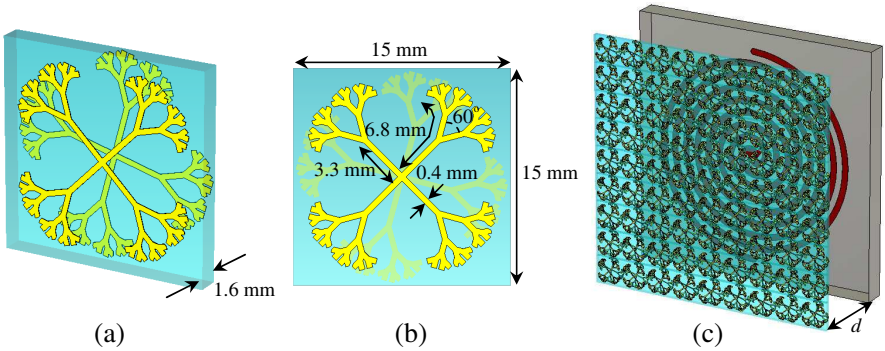

Figure 6. (a) Perspective view of the unit cell of dendritic fractal CMM structure. (b) Top view of the unit cell structure with its geometric parameters. (c) Configuration of the cavity backed ARSPL antenna with the planar scaled (with scale factor of 0.6) dendritic fractal CMM cover.

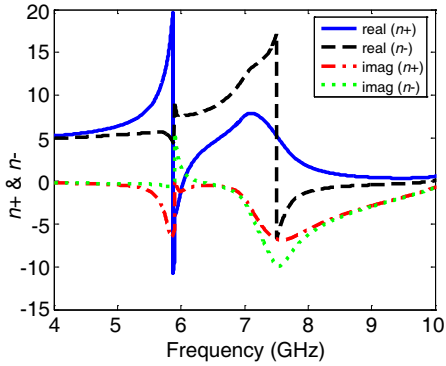

Figure 7. The real and imaginary parts of the RCP and LCP refractive indices for the planar scaled (with scale factor of 0.6) dendritic fractal CMM structure.

range of 4 GHz to 10 GHz, the real and imaginary parts of $n_{\pm}$ are calculated and illustrated in Figure 7. With attention to these results, it is expected that the frequency of about 5.9 GHz is appropriate for focusing electromagnetic waves and achieving directive emission.

4.2. Simulated Results

A 9×9 array of planar scaled dendritic fractal unit cells (with scale factor of 0.6) is placed at a distance d from the ARSPL antenna with

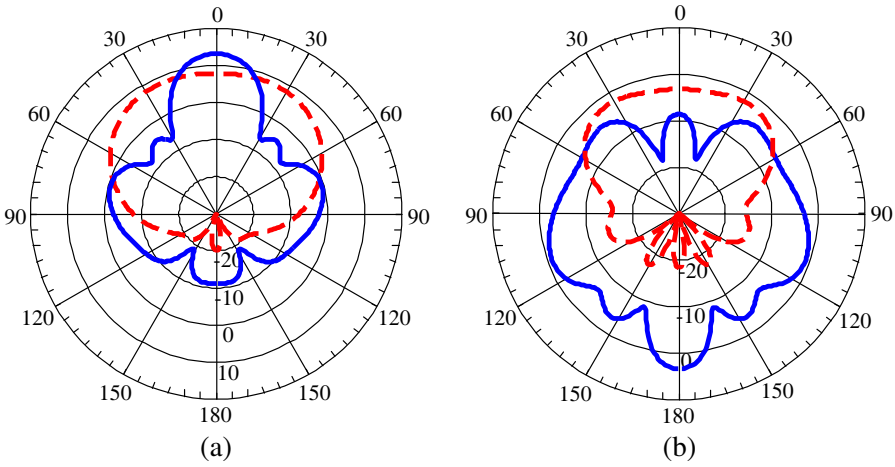

Figure 8. The radiation patterns (in dB) of cavity backed ARSPL antenna at frequency of 5.8 GHz with (solid line) and without (dashed line) planar scaled dendritic fractal CMM cover in $\varphi = 0°$ plane. (a) RHCP and (b) LHCP.

cavity dimensions of 81 mm × 81 mm × 7 mm, as shown in Figure 6(c). Numerical simulations executed in the frequency range 5.5 GHz to 6.5 GHz shows that the optimum value of d is about 25.5 mm. It can be seen that the obtained frequency from optimization process (i.e., 5.8 GHz) is very close to the initial value of frequency obtained from the retrieved results. Such a consistency is certainly due to the use of a CMM cover consisting of many unit cells. Theoretically, the maximum gain of an aperture antenna with the same transverse dimensions as ARSPL antenna at frequency of 5.8 GHz is $4\pi A/\lambda^2 = 15$ dB. The radiation patterns in the $\varphi = 0°$ plane at 5.8 GHz for the ARSPL antenna with and without dendritic fractal CMM cover are shown in Figure 8. Observe that the RCP gain of ARSPL antenna with cover is about 23 dB higher than its LCP gain in the boresight direction ($\theta = 0°$). Also, the HPBW of antenna with cover is about 25° while the common antenna without cover has a HPBW of about 101°.

The RCP gain and AR in the boresight direction ($\theta = 0°$), and S_{11} of ARSPL antenna with and without CMM cover in the frequency range of 5.9 GHz to 6.5 GHz are shown in Figure 9. Here, the RCP gain of ARSPL antenna with cover approaches 13.5 dB at frequency 5.8 GHz, while the common antenna without cover has a gain of 8 dB. Observe that due to the absence of absorbing strip in the metallic cavity, AR of common antenna without cover is higher than 3 dB, but

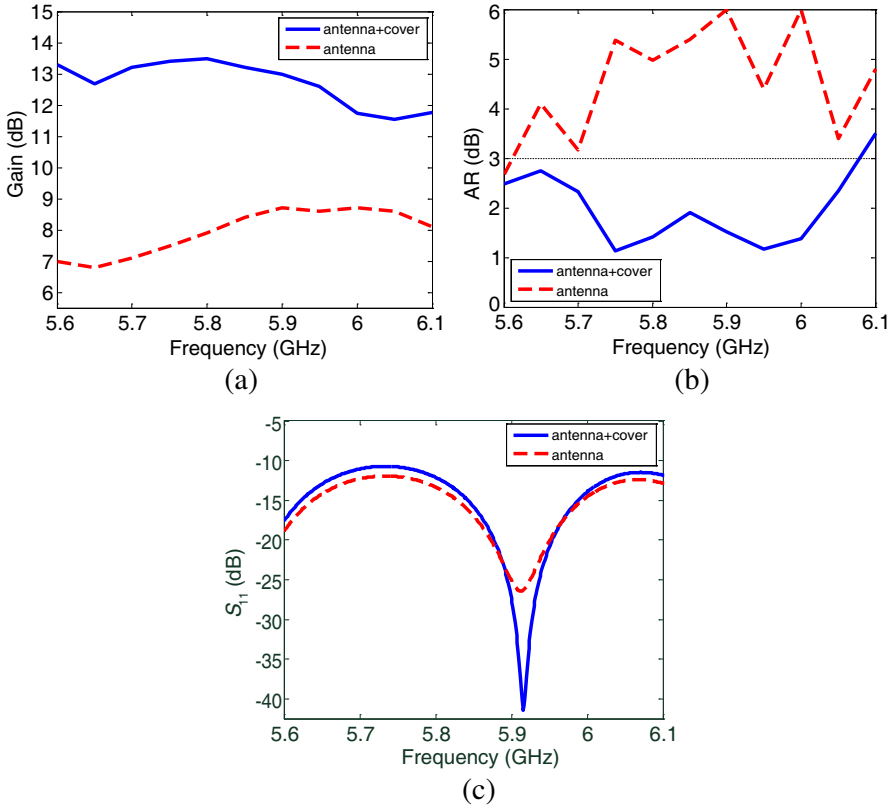

Figure 9. (a) The simulated RCP gain, (b) AR and (c) S_{11} of the cavity backed ARSPL antenna with and without planar scaled dendritic fractal CMM cover.

with the addition of CMM cover AR is significantly decreased. Also, the RCP gain of antenna with the CMM cover is increased by about 3–6.3 dB.

5. HELICAL ANTENNA WITH TWISTED CROSSES CMM COVER

5.1. Antenna Design

The geometrical configuration of the helical antenna is shown in Figure 10(a). This is a relatively simple non-planar traveling wave type antenna consisting of a conducting wire wound in the form of a screw, usually backed by a ground plane or shaped reflector and

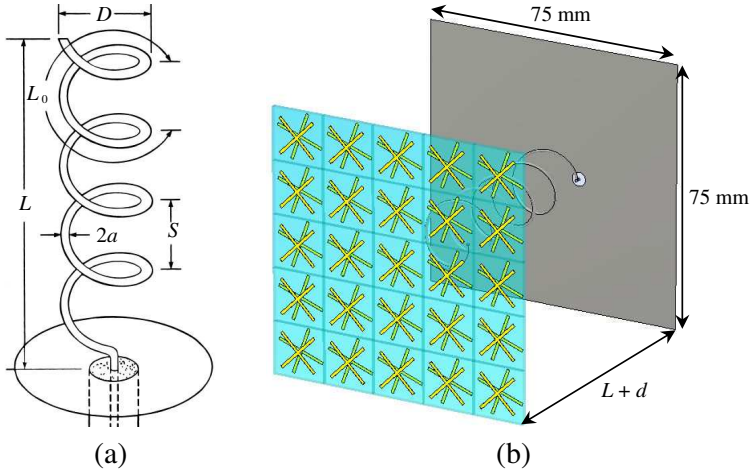

Figure 10. (a) Helical antenna with ground plane. (b) Configuration of the helical antenna with the twisted crosses CMM cover.

driven by an appropriate feed. The most common design is a single wire backed by a ground and fed by a coaxial line. The axial mode of operation occurs when the circumference of helix is in the order of one wavelength. The most important parameters of a helix are the beam width, gain, impedance and axial ratio as given by formulas in Ref. [46] in terms of N (the number of turns), C (the circumference) and S (the spacing between two turns). In this section, an axial mode helical antenna at the frequency of about 6 GHz with geometrical parameters of $N = 5$, $D = 15.9\,\text{mm}$, $S = 11.55\,\text{mm}$, $a = 0.5\,\text{mm}$ and axial length $L = 58\,\text{mm}$ is considered.

5.2. Placement of CMM Cover and Simulated Results

A 5×5 array of twisted crosses unit cells is located at a distance $L + d$ from the antenna ground plane with dimensions $75\,\text{mm} \times 75\,\text{mm}$, as shown in Figure 10(b). Numerical simulations performed in the frequency range 5.5 GHz to 6.5 GHz show that the optimized value of d is about 23 mm. The RCP gain of antenna with CMM cover approaches 14.1 dB at 6 GHz, while the common antenna without cover has RCP gain of 11.5 dB. Note that the maximum gain of an aperture antenna with the same transverse dimension of the proposed antenna is 14.5 dB. The radiation patterns in the $\varphi = 0^\circ$ plane and at frequency of 6 GHz for the helical antenna with and without CMM cover are shown in Figure 11. The radiation patterns of the proposed antenna

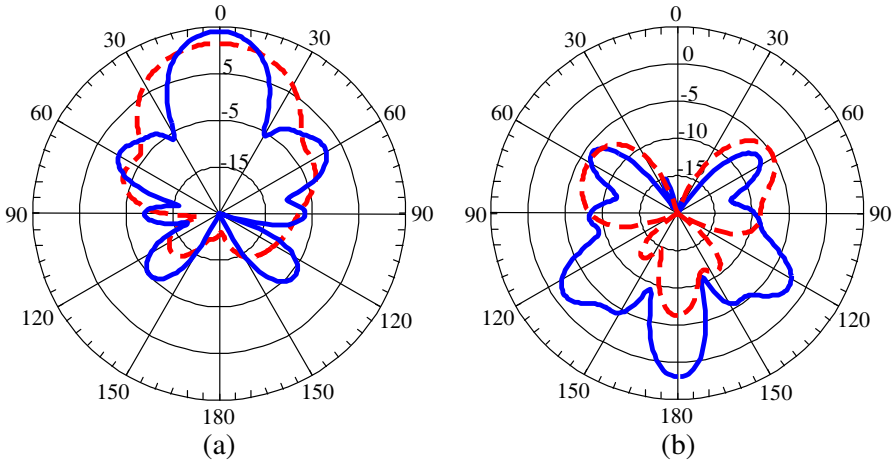

Figure 11. Radiation patterns of helical antenna (in dB) at frequency of 6 GHz with (solid line) and without (dashed line) twisted crosses CMM cover in $\varphi = 0°$ plane. (a) RHCP. (b) LHCP.

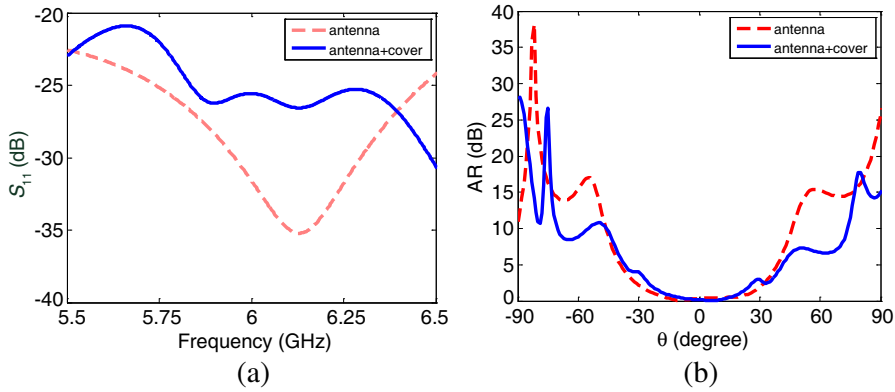

Figure 12. (a) Simulated S_{11}, and (b) AR of the helical antenna with and without twisted crosses CMM cover.

in the $\varphi = 0°$ and $\varphi = 90°$ planes are almost the same. The RCP gain of helical antenna with cover in the boresight direction ($\theta = 0°$) is about 40 dB higher than its LCP gain. Also, the HPBW and SLL of helical antenna with cover are 26° and -13 dB, while the common helical antenna without cover has HPBW and SLL of 49° and -14 dB, respectively. AR as a function of θ, and S_{11} of ARSPL antenna (with the feed impedance of 100 Ω) with and without CMM cover in

the frequency range 5.5 GHz to 6.5 GHz are illustrated in Figure 12. Note that AR of antenna with CMM cover in the boresight direction approaches 0.17 dB.

It should be noticed that the dendritic fractal CMM structure proposed in Section 4.1 can be also utilized in this antenna structure.

6. CONCLUSIONS

A novel technique based on the chiral metamaterial (CMM) structures for enhancing the gain and improving the axial ratio (AR) of circularly polarized (CP) antenna is presented and investigated by numerical simulations. Two CMM structure were used as covers for planar Archimedean spiral (ARSPL) and non-planar helical antennas. The results show that the gain and AR of antennas can be significantly improved with the addition of the CMM covers in a proper place over the antenna, so that CP antenna gain almost approaches the theoretical limit of antenna gain. Gain of the cavity backed ARSPL antenna with the twisted crosses and the dendritic fractal CMM covers increased by about 5.5 dB at 5.9 GHz. Also, the gain of helical antenna with the twisted crosses cover increased by about 2.6 dB at 6 GHz. The results show that the best location for placing semi-planar CMM covers is about a half wavelength distance above the CP antenna at frequency of the best radiation characteristics are achieved. Thus, this criterion can be considered to select an initial value for optimization process.

REFERENCES

1. Semichaevsky, A. and A. Akyurtlu, "Homogenization of metamaterial-loaded substrates and superstrates for antennas," *Progress In Electromagnetics Research*, Vol. 71, 129–147, 2007.
2. Singh, G., "Double negative left-handed metamaterials for miniaturization of rectangular microstrip antenna," *Journal of Electromagnetic Analysis & Applications*, Vol. 2, 347–351, 2010.
3. Lee, J. and Y. Hao, "Characterization of microstrip patch antennas on metamaterial substrates loaded with complementary split-ring resonators," *Microwave Opt. Tech. Lett.*, Vol. 50, No. 8, Aug. 2008.
4. Alu, J., F. Bilotti, N. Engheta, and L. Vegni, "Subwavelength compact, resonant patch antenna loaded with metamaterials," *IEEE Trans. Antennas Propag.*, Vol. 55, No. 1, Jan. 2007.
5. Li, L.-W., Y.-N. T. S. Yeo, J. R. Mosig, and O. J. F. Martin,

"A broadband and high-gain metamaterial microstrip antenna," *Appl. Phys. Lett.*, Vol. 96, 164101, 2010.

6. Chaimool, S., K. L. Chung, and P. Akkaraekthalin, "Simultaneous gain and bandwidths enhancement of a single-feed circularly polarized microstrip patch antenna using a metamaterial reflective surface," *Progress In Electromagnetics Research B*, Vol. 22, 23–37, 2010.
7. Griguer, H., E. Marzolf, H. Lalj, F. Riouch, and M. Drissi, "Patch antenna bandwidth enhancement through the use of metamaterials," *International Conference on Telecommunications, 2009, ICT'09*, 2009.
8. Enoch, S., G. Tayeb, P. Sabouroux, N. Guerin, and P. Vincent, "A metamaterial for directive emission," *Phys. Rev. Lett.*, Vol. 89, 2002.
9. Hu, J., et al., "A new patch antenna with metamaterial cover," *Zhejiang University SCIENCE A*, Vol. 7, 89–94, 2006.
10. Attia, H., L. Yousefi, M. S. Boybay, and O. M. Ramahi, "Enhanced-gain microstrip antenna using engineered magnetic superstrates," *IEEE Antennas Propag. Lett.*, Vol. 8, 2009.
11. Wu, B.-I., W. Wang, J. Pacheco, X. Chen, T. Grzegorczyk, and J. A. Kong, "A study of using metamaterials as antenna substrate to enhance gain," *Progress In Electromagnetics Research*, Vol. 51, 295–328, 2005.
12. Attia, H., L. Yousefi, and O. M. Ramahi, "Analytical model for calculating the radiation field of microstrip antennas with artificial magnetic superstrates theory and experiment," *IEEE Trans. Antennas Propag.*, Vol. 59, No. 5, May 2011.
13. Chen, K.-S., K.-H. Lin, and H.-L. Su, "Microstrip antenna gain enhancement by metamaterial radome with more subwavelength holes," *Asia Pacific Microwave Conference, 2009, APMC 2009*, 2009.
14. Xiao, X. and H. Xu, "Low refractive metamaterials for gain enhancement of horn antenna," *Journal of Infrared Milli Terahz Waves*, Vol. 30, 225–232, 2009.
15. Tretyakov, S., I. Nefedov, A. Sihvola, S. Maslovski, and C. Simovski, "Waves and energy in chiral nihility," *Journal of Electromagnetic Waves and Applications*, Vol. 17, No. 5, 695–706, 2003.
16. Dong, J., "Exotic characteristics of power propagation in the chiral nihility fiber," *Progress In Electromagnetics Research*, Vol. 99, 163–178, 2009.

17. Dong, J., J. Li, and F.-Q. Yang, "Guided modes in the four-layer slab waveguide containing chiral nihility core," *Progress In Electromagnetics Research*, Vol. 112, 241–255, 2011.
18. Naqvi, A., A. Hussain, and Q. A. Naqvi, "Waves in fractional dual planar waveguides containing chiral nihility metamaterial," *Journal of Electromagnetic Waves and Applications*, Vol. 24, Nos. 11–12, 1575–1586, 2010.
19. Dong, J. F. and C. Xu, "Surface polaritons in planar chiral nihility metamaterial waveguides," *Opt. Commun.*, Vol. 282, 3899–3904, 2009.
20. Tuz, V. R. and C.-W. Qiu, "Semi-infinite chiral nihility photonics: Parametric dependence, wave tunneling and rejection," *Progress In Electromagnetics Research*, Vol. 103, 139–152, 2010.
21. Naqvi, Q. A., "Fractional dual solutions in grounded chiral nihility slab and their effect on outside field," *Journal of Electromagnetic Waves and Applications*, Vol. 23, Nos. 5–6, 773–784, 2009.
22. Qamar, S. R., A. Naqvi, A. A. Syed, and Q. A. Naqvi, "Radiation characteristics of elementary sources located in unbounded chiral nihility metamaterial," *Journal of Electromagnetic Waves and Applications*, Vol. 25, Nos. 5–6, 713–722, 2011.
23. Ahmad, S. and Q. A. Naqvi, "Directive EM radiation of a line source in the presence of a coated nihility cylinder," *Journal of Electromagnetic Waves and Applications*, Vol. 23, Nos. 5–6, 761–771, 2009.
24. Pendry, J. B., "A chiral route to negative refraction," *Science*, Vol. 306, 1353–1354, 2004.
25. Mackay, T. G., "Plane waves with negative phase velocity in isotropic chiral mediums," *Microwave Opt. Tech. Lett.*, Vol. 45, No. 2, 120–121, 2005.
26. Zhao, R., T. Koschny, E. N. Economou, and C. M. Soukoulis, "Comparison of chiral metamaterial designs for repulsive Casimir force," *Phys. Rev. B*, Vol. 81, 235126, 2010.
27. Plum, E., J. Zhou, J. Dong, V. A. Fedotov, T. Koschny, C. M. Soukoulis, and N. I. Zheludev, "Metamaterial with negative index due to chirality," *Phys. Rev. B*, Vol. 79, 035407, 2009.
28. Zhou, J., J. Dong, B. Wang, T. Koschny, M. Kafesaki, and C. M. Soukoulis, "Negative refractive index due to chirality," *Phys. Rev. B*, Vol. 79, 121104, 2009.
29. Li, Z., R. Zhao, T. Koschny, M. Kafesaki, and C. M. Soukoulis, "Chiral metamaterials with negative refractive index based on four "U" split ring resonators," *Appl. Phys. Lett.*, Vol. 97, 081901,

2010.

30. Wu, Z., B. Q. Zhang, and S. Zhong, "A double-layer chiral metamaterial with negative index," *Journal of Electromagnetic Waves and Applications*, Vol. 24, No. 7, 983–992, 2010.
31. Zhao, R., L. Zhang, J. Zhou, T. Koschny, and C. M. Soukoulis, "Conjugated gammadion chiral metamaterial with uniaxial optical activity and negative refractive index," *Phys. Rev. B*, Vol. 83, 035105, 2011.
32. Li, Z., K. B. Alici, E. Colak, and E. Ozbay, "Complementary chiral metamaterials with giant optical activity and negative refractive index," *Appl. Phys. Lett.*, Vol. 98, 161907, 2011.
33. Li, Z., F.-Q. Yang, and J. Dong, "Design and simulation of L-shaped chiral negative refractive index structure," *Progress In Electromagnetics Research*, Vol. 116, 395–408, 2011.
34. Ye, Y. and S. He, "90° polarization rotator using a bilayered chiral metamaterial with giant optical activity," *Appl. Phys. Lett.*, Vol. 96, 203501, 2010.
35. Ye, Y., X. Li, F. Zhuang, and S.-W. Chang, "Homogeneous circular polarizers using a bilayered chiral metamaterial," *Appl. Phys. Lett.*, Vol. 99, 031111, 2011.
36. Illahi, A. and Q. A. Naqvi, "Study of focusing of electromagnetic waves reflected by a PEMC backed chiral nihility reflector using Maslov's method," *Journal of Electromagnetic Waves and Applications*, Vol. 23, No. 7, 863–873, 2009.
37. Jin, Y. and S. He, "Focusing by a slab of chiral medium," *Optics Express*, Vol. 13, No. 13, 4974–4979, 2005.
38. Monzon, C. and D. W. Forester, "Negative refraction and focusing of circularly polarized waves in optically active media," *Phys. Rev. Lett.*, Vol. 95, 123904, 2005.
39. Wang, B., T. Koschny, and C. M. Soukoulis, "Wide-angle and polarization-independent chiral metamaterial absorber," *Phys. Rev. B*, Vol. 80, 033108, 2009.
40. Cheng, Q., W. X. Jiang, and T. J. Cui, "Investigations of the electromagnetic properties of three-dimensional arbitrarily-shaped cloaks," *Progress In Electromagnetics Research*, Vol. 94, 105–117, 2009.
41. Luo, Y., J. Zhang, H. Chen, B.-I. Wu, and L.-X. Ran, "Wave and ray analysis of a type of cloak exhibiting magnified and shifted scattering effect," *Progress In Electromagnetics Research*, Vol. 95, 167–178, 2009.
42. Lindell, I. V., A. H. Sihvola, S. A. Tretyakov, and A. J. Viitanen,

Electromagnetic Waves in Chiral and Bi-isotropic Media, Artech House, Boston, 1994.

43. Serdyukov, A., I. Semchenko, S. Tretyakov, and A. Sihvola, *Electromagnetics of Bi-anisotropic Materials Theory and Applications*, Gordon and Breach Science Publishers, 2001.
44. Zhao, R., T. Koschny, and C. M. Soukoulis, "Chiral metamaterials: Retrieval of the effective parameters with and without substrate," *Optics Express*, Vol. 18, No. 14, Jul. 2010.
45. Balanis, C. A., *Modern Antenna Handbook*, John Wiley & Sons, 2008.
46. Kraus, J. D. and R. J. Marhefka, *Antennas: For All Applications*, 3rd edition, McGraw Hill, New York, 2001.